Monotonic CHF increase with enhanced wicked liquid volume rate on nanostructured surfaces

Namgook Kim[1], Hong Hyun Son[1], Sung Joong Kim[1,2*]

[1]*Department of Nuclear Engineering, Hanyang University*
[2]*Institute of Nano Science & Technology, Hanyang University*
222 Wangsimri-ro, Seongdong-gu, Seoul 04763, Republic of Korea
ngkim@hanyang.ac.kr, hhson@hanyang.ac.kr,
[*]*Corresponding author: sungjkim@hanyang.ac.kr*

1. Introduction

It has been found that wicking potential on nanostructures can enhance the CHF. Rahman et al. [1] reported that the CHF enhancement depends strongly on the wicked liquid volume rate, called wickability, by measuring the absorbed liquid rate in a capillary tube. Here, the wicked liquid volume rate needs to be separately investigated in light of the pore cross-sectional area and the wicking velocity because the particle size of nanostructures differently affects those parameters. For example, higher particle size increases the pore cross-sectional area while decreases the wicking velocity due to reduced capillary pressure.

In this regard, we here tried to measure the wicking velocity for various particle size. The CHF enhancement is individually compared with the particle size and the wicking velocity. Finally, the wicked liquid volume rate, combination of the pore cross-sectional area and the wicking velocity, showed linear relation with CHF enhancement.

2. Experiment

2.1 Sample preparation

Test samples, grade 304 Stainless steel, were prepared by three processes. Firstly to give the same initial roughness condition, the samples were ground with a grit-800 sandpaper and cleansed with an ethanol solution to remove any contaminants in this process. Later, the nanostructures were formed on the surface using DC sputtering of Cr target under the different substrate temperatures. The final step was the oxidation to change the Cr-sputtered nanostructures on the surface. The conditions used in the sputtering process and the oxidation process are listed in Table 1 and 2, respectively.

Table 1. Sputtering condition

Sputtering parameters	Sputtering condition
Target material	Cr
Power (W)	150~160
Gas pressure (torr.)	1.0×10^{-2}
Substrate temperature (°C)	150 / 300 / 600

Table 2. Oxidation condition

Oxidation parameter	Oxidation condition
Temperature (°C)	400
Time (days)	20

All the test surfaces used in this study are listed in Table 3 following these three processes of the sample preparation. Here, *B* refers to 'bare', *Cr* refers to 'Cr-sputtered', *T150* refers to 'sputtered at substrate temperature of 150 °C', and *Ox* refers to 'Oxidation'. For example, *OxCr-T600* refers to the oxidized test surface sputtered at the substrate temperature of 600 °C.

Table 3. Test matrix

Surface condition	Cr-sputtered surface	Cr-sputtered surface with oxidation
Bare	Bare	-
150°C substrate temperature	Cr-T150	OxCr-T150
300°C substrate temperature	Cr-T300	OxCr-T300
600°C substrate temperature	Cr-T600	OxCr-T600

2.2 Experimental setup

A schematic of the pool boiling apparatus and a design of the test section are shown in Fig. 1. The length, width, and thickness of the test sample were 45, 10, and 2 mm, respectively. Heat transfer area was 25 mm×10 mm = 250 mm^2. Polyether ether ketone (PEEK) and epoxy were used for thermal and electrical insulations. Three K-type thermocouples ware attached underneath the samples to measure inner wall temperature (Fig. 1(c)). Voltage taps were attached to the PEEK screw at each side to measure voltage drop.

Direct Joule heating method was used to carefully supply steady state heat flux. Applied heat flux was calculated by

$$q'' = \frac{Power}{A_{heated}} = \frac{VI}{WL_{heated}} \quad (1)$$

Here, V is the measured voltage drop across the test material, I is the measured current, W is the width of the

heat transfer area, and L_{heated} is the heated length. Uncertainty of the measured heat flux was estimated as 5.2% based on the error propagation method.

The Krüss EasyDrop instrument coupled with the high speed camera (Phantom v7.3) was used to quantify the dynamic wetting behavior of the test samples (Fig. 2). The frame rate of high speed camera was 2000 fps. After a water droplet was generated at the tip of syringe needle of wetting equipment, the contact diameter was measured over time from the moment the water droplet contact with the sample surface while gradually raising the substrate on which the sample was placed.

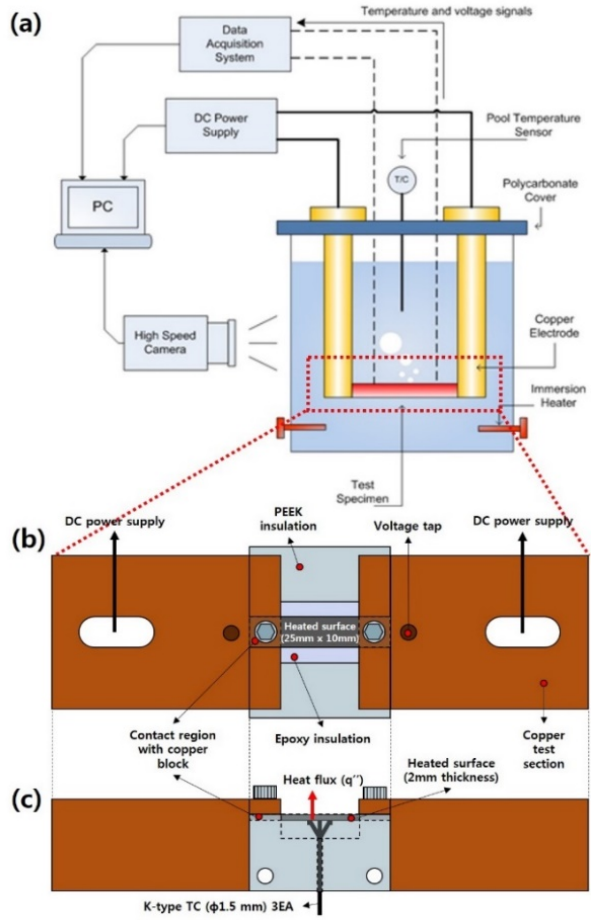

Fig. 1. Schematic diagram of (a) pool boiling apparatus; (b) upper side test section; (c) lateral side test section.

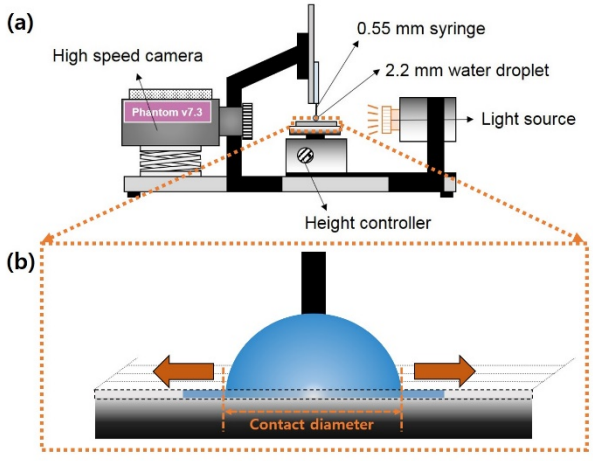

Fig. 2. Schematic diagram of (a) dynamic wetting measurement instrument; (b) water droplet behavior on the test samples.

3. Result and discussion

3.1 Sample characterization

Fig. 3 shows the surface morphology of (a) Cr-T150, (b) OxCr-T150, (c) Cr-T30, (d) OxCr-T300, (e) Cr-T600, and (f) OxCr-T600 using NOVA NANO SEM 450. There is the particulate nanostructures caused by the Cr sputtering process (Fig. 3(a), (c), and (e)). The nanostructures on the oxidized surfaces became larger than the Cr-sputtered particulate nanostructures (Fig. 3(b), (d), and (f)). This growth of the particulate nanostructures could be confirmed by measuring the particle sizes in SEM images. The size of nanostructures on Cr-T150, Cr-T300, and Cr-T600 are 244, 169, and 164 nm, respectively. On the other hand, the nanostructure sizes of OxCr-T150, OxCr-T300, and OxCr-T600 are 300, 186, and 180 nm, respectively.

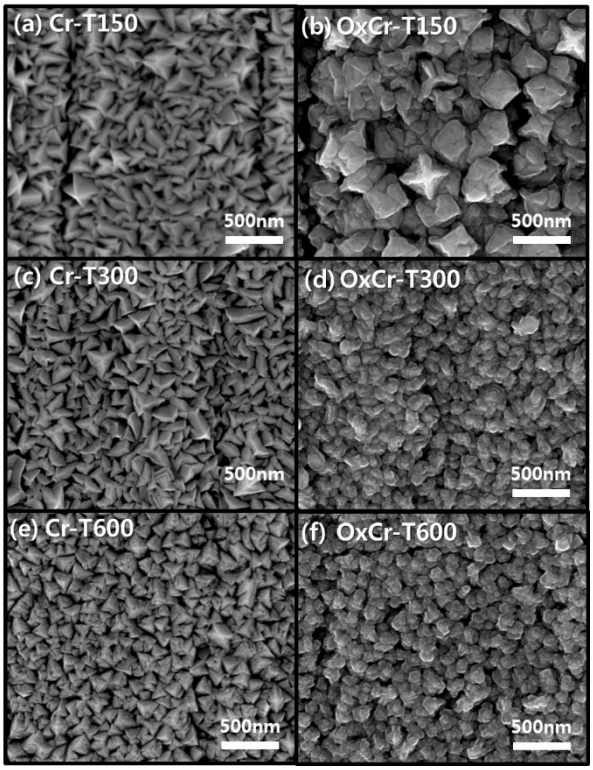

Fig. 3. SEM images of surface morphology: (a) Cr-T150; (b) OxCr-T150; (c) Cr-T300; (d) OxCr-T300; (e) Cr-T600; (f) OxCr-T600.

3.2 Critical Heat Flux

In this study, pool boiling experiment was conducted to measure the CHF of each surfaces. CHF was determined as the heat flux at the time of temperature jump.

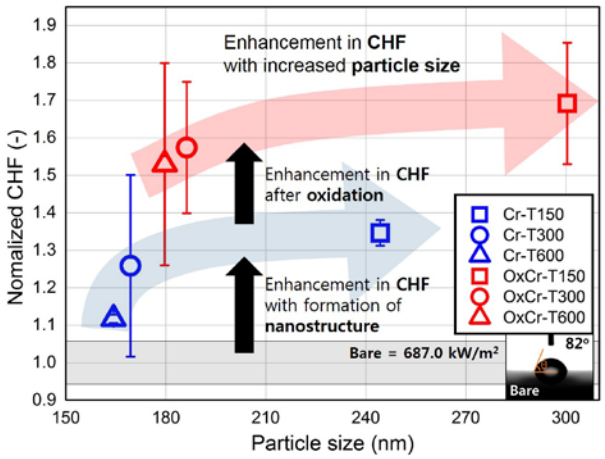

Fig. 4. Normalized CHF of test surfaces according to the particle size of nanostructures.

Figure 4 shows that CHF was enhanced with an increase of particle size. The CHF of bare surface was measured much lower than Zuber's prediction [2], which is 1072 kW/m^2. This is because the bare surface had the high contact angle of 82^o in which Kandlikar's prediction [3] gives approximately 748 kW/m^2. In addition, the repeatability of CHF values seems weak for Cr-T300 and OxCr-T600, although averaged CHF shows monotonic increase trend. Nevertheless, more CHF experiments are needed to obtain reliable CHF trends. The CHF enhancement ratio of Cr-T150, Cr-T300, and Cr-T600 is 34.6 %, 25.9 %, and 11.7 %, respectively. Moreover, CHF of OxCr-T150, OxCr-T300, and OxCr-T600 was much increased by 69.2 %, 57.4 %, and 52.9 %, respectively. Importantly, the enhancement in CHF of OxCr-T300 and -T600 was higher than that of Cr-T150, although the particle size was smaller. Therefore, particle size alone is not enough to evaluate CHF enhancement, so it is necessary to explore another parameter affecting the enhancement in CHF.

3.3 Dynamic wetting

The nanostructures has a wicking potential, which could contribute to enhancement in CHF. In this study, the dynamic wetting behavior was evaluated to reveal the relation between the wickability and CHF enhancement. Fig. 5 shows the increasing contact diameter of each samples as a function of time, which is a sort of the dynamic wetting phenomenon. The spreading velocity is quantified on the basis of the slope of increasing contact diameter.

As shown in Fig. 5(a), all of the contact diameters increased following the spreading time and spreading velocity is sharply reduced after about 12ms. This is because the spreading behavior is dominant until the water droplets contact the surfaces of test sample however the wicking behavior on nanostructured surface is dominant since then. In this study, therefore, the spreading velocity was measured at the spreading time from 25ms to 35ms considered as showing stabilized wicking behavior. The measured spreading velocities of

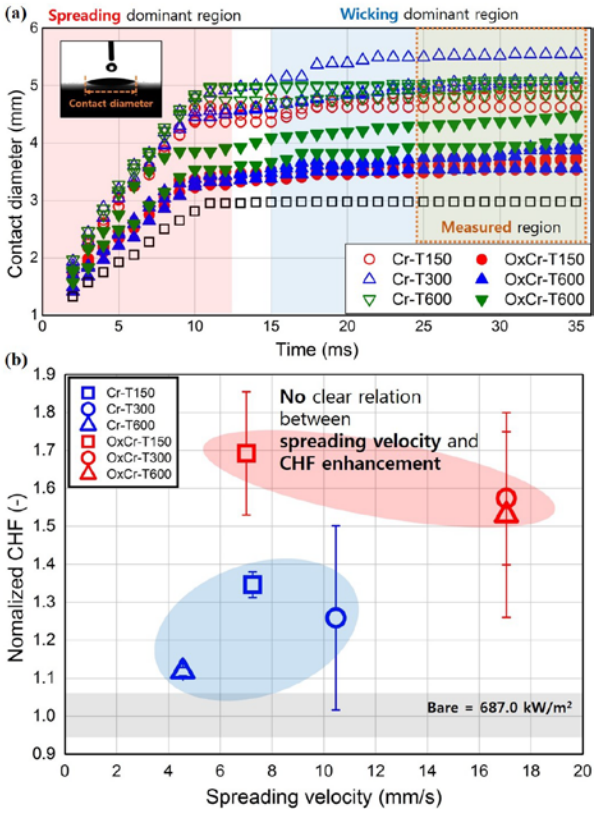

Fig. 5. Quantification of spreading velocity: (a) dynamic wetting behavior; (b) Normalized CHF of test surfaces according to the spreading velocity.

Cr-T150, Cr-T300, Cr-T600, OxCr-T150, OxCr-T300, and OxCr-T600 were 7.26, 10.47, 4.55, 7.01, 17.05, and 17.51 mm/s, respectively.

Then, measured spreading velocity was compared with the normalized CHF of each surfaces as shown in Fig. 5(b). The spreading rate was increased with both Cr-sputtered process and oxidation process. However, there was no clear relation between the spreading velocity and CHF enhancement.

3.3 Microlayer evaporation mechanism

Recently, the researches to understand the pool boiling CHF mechanism have focused on the microlayer evaporation mechanism. In this mechanism, the liquid inflow driven by the capillary pressure is sucked into the microlayer around dry spots and delays the formation of dry patches (Fig. 6). Thus, enhanced wicked liquid inflow, which can compensate more evaporative heat, effectively delays the formation of irreversible dry patches. In this approach, the enhancement of CHF, i.e. $q''_{enh.}$, by wicked liquid inflow can be expressed as the following equation (Eq. (2)).

$$q''_{enh.} = \frac{\dot{m}_f h_{fg}}{A_t} = \frac{\rho_f u_w A_c h_{fg}}{A_t} \propto A_c u_w \tag{2}$$

$$A_c = \bar{D}_p^2 \left(\frac{\sqrt{3}}{4} - \frac{\pi}{8}\right) \tag{3}$$

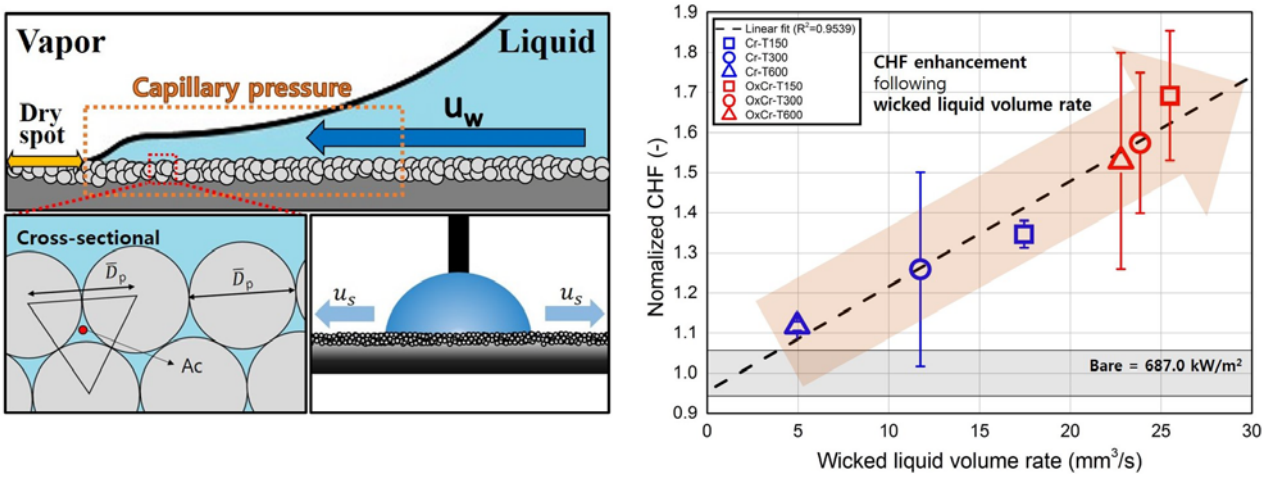

Fig. 6. Schematic figure of microlayer evaporation model and normalized CHF according to the wicked liquid volume rate.

$$u_w \propto u_s \tag{4}$$

$$q''_{enh.} \propto A_c u_w \propto \bar{D}_p^2 u_s \left(\frac{\sqrt{3}}{4} - \frac{\pi}{8}\right) = \dot{\bar{V}}_w \tag{5}$$

where $\dot{m}_f$ is the mass flux of wicked liquid inflow, h_{fg} is the latent heat from liquid to gas, A_c and A_t is the cross-sectional area of wicked channel and the heat transfer area, ρ_f is the density of liquid, u_w and u_s is the wicking and spreading velocity, and $\bar{D}_p$ is the average diameter of the particulate nanostructures . Here, wicked channel refers the space between the nanostructures. If it is assumed that the particulate nanostructures have a complete circle shape and are uniformly distributed, A_c is proportional to the square of $\bar{D}_p$ (Eq. (3)). And it is assumed that u_w is proportional to the u_s measured by the dynamic wetting test in this study, because both velocities are associated with the capillary pressure (Eq. (4)). So, the wicked liquid volume rate, i.e. $\dot{\bar{V}}_w$, which is the product of square average particle diameter and the spreading velocity, is the only factor affecting the CHF enhancement when assumed that other parameters were not changed (Eq. (5)).

The calculated wicked liquid volume rate showed linear relation with CHF enhancement ratio, which has high r square of about 0.95. This result is well matched with the study of Rahman et al.[1] and Ahn et al.[4]

4. Conclusions

Pool boiling experiments were conducted with grade 304 stainless steel samples sputtered by Cr at substrate temperature of 150 ºC, 300 ºC, and 600 ºC before and after oxidation at 400 ºC during 20 days. In this study, the effect of the wicked liquid volume rate, which is the product of the square average particle diameter and the spreading velocity, on enhancement in CHF was analyzed according to the microlayer evaporation mechanism. As a result, it is confirmed that there is a linear relation between the wicked liquid volume rate and CHF enhancement, although the effect of the spreading velocity on CHF enhancement is not clear.

Acknowledgement

This research was supported by the Basic Science Research Program through the National Research Foundation of Korea (NRF) funded by the Ministry of Science, ICT & Future Planning (No. NRF-2015R1C1A1A01054861), and by the National Research Foundation of Korea (NRF) grant funded by the Korean government (MSIP: Ministry of Science, ICT and Future Planning) (No. NRF-2017M2A8A5018575)

REFERENCES

[1] M.M.Rahman, Role of Wickability on the Critical Heat Flux of Structured Superhydrophilic Surfaces, Langmuir Volume: 30 Issue 37, 2014, 0743-7463
[2] N.Zuber, AECU-4439, 1959
[3] S.G.Kandlikar, A Theoretical Model to Predict Pool Boiling CHF Incorporating Effects of Contact Angle and Orientation, Journal of Hear Transfer 123, 2001, 1071-1079
[4] H.S.Ahn, The effect of capillary wicking action of micro/nano structures on pool boiling critical heat flux, International Journal of Heat and Mass Transfer 55, 2012, 89-92
[5] H.H.Son, Capillary wicking effect of a Cr-sputered superhydrophilic surface on enhancement of pool obiling critical heat flux, International Journal of Heat and Mass Transfer 113, 2017, 115-128.